Atomistic simulations of nanotube fracture

T. Belytschko,* S. P. Xiao, G. C. Schatz, and R. S. Ruoff
Department of Mechanical Engineering, 2145 North Sheridan Road, Northwestern University, Evanston, Illinois 60208
(Received 10 October 2001; published 20 June 2002)

The fracture of carbon nanotubes is studied by molecular mechanics simulations. The fracture behavior is found to be almost independent of the separation energy and to depend primarily on the inflection point in the interatomic potential. The fracture strain of a zigzag nanotube is predicted to be between 10% and 15%, which compares reasonably well with experimental results. The predicted range of fracture stresses is 65–93 GPa and is markedly higher than observed. The computed fracture strengths of chiral and armchair nanotubes are above these values. Various plausible small-scale defects do not suffice to bring the failure stresses into agreement with available experimental results. As in the experiments, the fracture of carbon nanotubes is predicted to be brittle.

DOI: 10.1103/PhysRevB.65.235430 PACS number(s): 61.46.+w, 81.07.De

I. INTRODUCTION

We report here molecular mechanics and molecular dynamics studies of the failure of nanotubes. Nanotubes, since their discovery in 1991,[1] have attracted much interest because of their ability to sustain large deformations and their great stiffness and possible high strength. The ability of carbon nanotubes to sustain large bending deformations has been observed experimentally and verified by molecular dynamics studies.[2–4] Molecular dynamics studies have also replicated the ability of nanotubes to sustain very distorted configurations with only elastic deformations and no creation of atomic defects.[2,3,5,6]

Previous molecular mechanics simulations predict that ideal single-walled carbon nanotubes (SWNT's) should possess extremely high tensile strengths. The strain at tensile failure has been predicted to be as high as ~30% for SWCNT's (Ref. 7) by molecular mechanics. However, in the only experimental measurement[8] reported so far, the tensile failure strain is usually between ~10% and ~13% and as low as 2%. A recent study[9] of SWCNT's with the tight-binding approximation describes a mechanism of defect nucleation in which two hexagon pairs are converted, through a Stone-Wales bond rotation, into 5/7/7/5 (pairs of pentagon-heptagon) defects. It was hypothesized that at high temperatures, plastic response may occur due to separation and glide of these 5/7/7/5 defects whereas at lower temperature their presence may result in fracture.[9–11]

Molecular simulations of fracture are now quite commonplace. The earliest atomistic simulations of fracture were reported in the early 1970s[12–14] and many materials have been investigated. Works closely related to this are of Shenderova *et al.*[15] who examined the fracture of polycrystalline diamond, and of Omeltchenko *et al.*[16] who studied notched graphene.

In this paper, the fracture of carbon nanotubes is studied by molecular mechanics and dynamics. We show that some of the features of the experimental results of Yu *et al.*[8] on the failure of carbon nanotubes can be reproduced reasonably well by molecular mechanics: the predicted failure strains are 10–16% which agrees with some of the experimental results. The predicted failure stress for a defect-free nanotube is 65–93 GPa, which is significantly above that for all but one of the specimens measured. Furthermore, we show that some of the scatter of failure strains reported by Yu *et al.*[8] can be partially explained by the presence of defects and variations due to chirality. The simulations always exhibit brittle fracture, which also agrees with these experiments.

Nanotubes are particularly attractive for studying fracture by molecular mechanics because they are single molecules with all atoms joined by identical bonds. Thus the degree of heterogeneity and the variety of length scales found in fracture of most materials at the macro scale is probably absent in nanotubes. The major defect that has been postulated is the previously mentioned Stone-Wales defect that is of the order of several bonds. In addition, in experiments performed in the transmission electron microscope environment, it is possible for single atoms to be ejected by impact, see Smith and Luzzi[17] and Banhart.[18]

Of course, the interpretation of fracture simulations by atomistic models must be treated with care, since the reconfiguration of bonds is not taken into account. However, we show that for small initial defects, the fracture strength depends primarily on the inflection point of the interatomic energy and is almost independent of the dissociation energy. Since the inflection strain occurs substantially before the strain associated with bond breaking, where the formation of other bonds is expected, these results may give the correct picture of fracture at moderate temperatures (0–500 K).

II. COMPUTATIONAL METHODS

We used standard molecular mechanics and molecular dynamics methods. By molecular mechanics, we refer to methods where the equilibrium configuration of the model system is sought by minimizing the energy, which consists of the sum of the interatomic potentials minus any work by external forces. Such methods imply a temperature of 0 K and cannot account for the effects of temperature. In molecular dynamics methods, the momentum equations are integrated in time for the system of atoms with interatomic forces given by the interatomic potential. Thus the effects of nonzero temperatures are included, although there are always limitations of such predictions due to the statistical nature of molecular

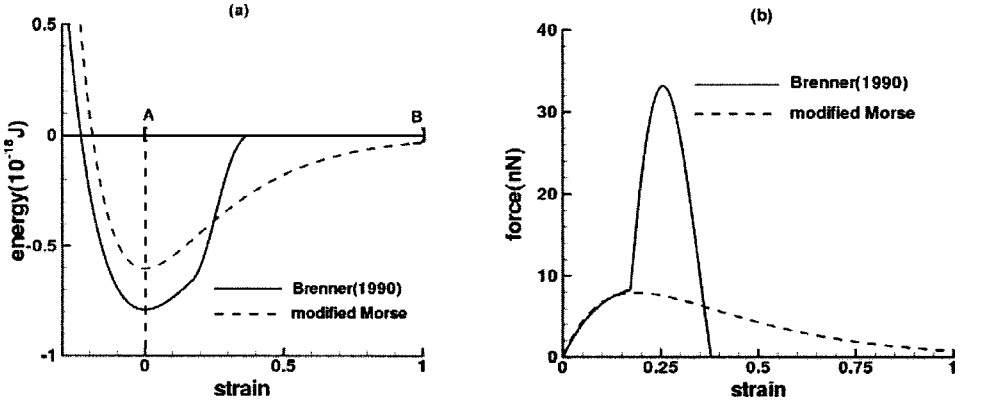

FIG. 1. The Brenner and modified Morse potentials and tensile force fields. (a) potential field for Brenner and modified Morse potential (b) force fields in segment [*AB*] in part (a).

motion for systems of bonded atoms and the brevity of the time scales that can be simulated as compared to the experimental time scales.

The interatomic bonds in nanotubes are hybridized sp^2 bonds. In most of our calculations, the interatomic potential is a modified Morse potential function in which a bond-angle-bending potential is added,

$$E = E_{\text{stretch}} + E_{\text{angle}}, \tag{1}$$

$$E_{\text{stretch}} = D_e\{[1 - e^{-\beta(r-r_0)}]^2 - 1\}, \tag{2}$$

$$E_{\text{angle}} = \tfrac{1}{2}k_\theta(\theta - \theta_0)^2[1 + k_{\text{sextic}}(\theta - \theta_0)^4], \tag{3}$$

where E_{stretch} is the bond energy due to bond stretch, E_{angle} is the bond energy due to bond angle-bending, r is the length of the bond, and θ is the current angle of the adjacent bond, a standard deformation measure in molecular mechanics. The parameters are

$$r_0 = 1.39\times10^{-10}\ \text{m}, \quad D_e = 6.031\,05\times10^{-19}\ \text{N m},$$

$$\beta = 2.625\times10^{10}\ \text{m}^{-1},$$

$$\theta_0 = 2.094\ \text{rad}, \quad k_\theta = 0.9\times10^{-18}\ \text{N m/rad}^2,$$

$$k_{\text{sextic}} = 0.754\ \text{rad}^{-4}.$$

This choice of parameters corresponds to a separation (dissociation) energy of 124 kcal/mol (5.62 eV/atom). This is the usual Morse[19] potential except that the bond angle-bending energy has been added and the constants are slightly modified so that it corresponds with the Brenner potential for strains below 10%.

The bond-angle-bending potential does not contribute to the stretching energy. It is added to stabilize the molecular structure in the tubular configuration. Without a bond-angle-bending energy, a stable configuration cannot be found for the nanotube. Instead, it tends to collapse onto itself. Thus the bond-angle-bending potential plays an essential role in establishing an equilibrium configuration of the nanotube; however, it has little effect on fracture.

The Brenner potential function[19] is generally considered more accurate and it is also more versatile than the Morse potential (it can handle bond hybridization and bonds with atoms other than carbon). It is given by

$$E_{ij} = \frac{1}{2}\sum_{j(\neq i)}[V_R(r_{ij}) - \overline{B}_{ij}V_A(r_{ij})], \tag{4}$$

where $\overline{B}_{ij}$ is a function of bond angle and

$$V_R(r_{ij}) = f(r_{ij})\frac{D_e}{S-1}e^{-\sqrt{2S}\beta(r-r_e)},$$

$$V_A(r_{ij}) = f(r_{ij})\frac{D_eS}{S-1}e^{-\sqrt{(2/S)}\beta(r-r_e)}.$$

The function $f(r_{ij})$ restricts the pair potential to nearest neighbors and is called a cutoff function. It is given by

$$f(r) = \begin{cases} 1 & r < r_1 \\ \dfrac{1}{2}\left\{1 + \cos\left[\dfrac{\pi(r-r_1)}{r_2 - r_1}\right]\right\} & r_1 \leqslant r \leqslant r_2 \\ 0 & r > r_2, \end{cases} \tag{5}$$

where

$$r_0 = 1.4507\times10^{-10}\ \text{m}, \quad D_e = 9.648\times10^{-19}\ \text{N m},$$

$$\beta = 2.1\times10^{10}\ \text{m}^{-1},$$

$$S = 1.22, \quad r_1 = 1.7\times10^{-10}\ \text{m}, \quad r_2 = 2.0\times10^{-10}\ \text{m}.$$

Figure 1 compares the interatomic stretching energy and force for the Brenner and the modified Morse potentials in the tensile regime. Because the stretching energy dominates the behavior in fracture, we show the relationships between force and bond strain with the bond angle kept constant. Strain is denoted by ε and is defined by $\varepsilon = (l - l_0)/l_0$ where l_0 is the equilibrium (initial) length and l the current length of the bond (i.e., the distance between nuclei). In the Brenner potential, the cutoff function $f(r_{ij})$ introduces a dramatic increase in the interatomic force at $r = r_1$ (like a camelback on the force curve), which rises sharply with a peak at around 30% strain. This strange feature in the force is a result of the cutoff function on the interatomic potential. Shenderova *et al.*[15] also noted this behavior and shifted the cutoff function to larger strains (specific values are not given) so that it occurs after the inflection point in the interatomic potential. We have found that the cutoff affects fracture behavior even when it is shifted to 100% strain.

We have compared the stress-strain response, i.e., the elastic modulus or Young's modulus, of zigzag nanotubes for this modified Morse potential to various experimental and numerical results in the literature. In examining values of the elastic modulus, it should be borne in mind that the axial response of a nanotube is quite nonlinear between its unstressed equilibrium configuration and the configuration preceding fracture. Therefore, we give both the tangent modulus and secant moduli for various strain levels. The tangent modulus E is the slope of the stress-strain curve, and unless specified otherwise, it refers to the slope at zero strain in this paper. The secant modulus E_{sec} is defined at a given value of strain $\bar{\varepsilon}$ by

$$E_{\text{sec}}=\frac{\sigma(\bar{\varepsilon})-\sigma(0)}{\bar{\varepsilon}}.$$

For our model, the tangent modulus is 1.16 TPa, the secant moduli at 5% and 10% strains are 0.85 and 0.74 TPa, respectively; Poisson's ratio $\nu=0.29$. These values are comparable to those obtained with a molecular mechanics simulation of a nanotube with the Brenner potential function: $E=1.07$ TPa and $\nu=0.19$.[3] Van Lier *et al.*[20] obtained $E=1.14$ TPa, $\nu=0.11$ with a Hartree-Fock 6-31G* calculation on a 150 atom [9,0] nanotube. Lu[21] obtained $E=0.97$ TPa and $\nu=0.28$ with an empirical force-constant model. Salvetat *et al.*[22] measured $E=0.81\pm0.41$ TPa. It was not specified whether these are tangent or secant moduli. Thus our values fall in the range of these computed and experimental values. It is noteworthy that our calculations show moderately large differences between the tangent modulus and the secant moduli. The separation (dissociation) energy of this Morse potential is 124 kcal/mol, which corresponds to the benzene carbon-carbon bond.

Certain qualitative and quantitative features of the interatomic force curve play key roles in fracture behavior. The strain at which the tensile force achieves its peak will be called the inflection strain since it corresponds to an inflection point in the potential. The interatomic force at this point will be called the peak force. The strain at which the tensile force vanishes is called the bond-breaking strain. The separation or bond-breaking energy (also called the dissociation energy) is the area under the force-strain curve (multiplied by the initial length), and it also corresponds to the change in the potential.

III. RESULTS

In the experiments of Yu *et al.*,[8] arc-grown multiwalled nanotubes were used. The experimental setup is shown in Fig. 2. The multiwalled nanotubes are attached to opposing atomic force microscope (AFM) cantilever tips by a solid carbonaceous material deposited onto the tips. In most cases, only the outer shell (the outer nanotube) was attached to the cantilever. The multiwalled nanotubes failed in a sheathlike pattern with typically only the outer nanotube failing. Therefore, only the outer nanotube was modeled in these studies. Any interactions of the outer nanotube with the inner tubes were neglected.

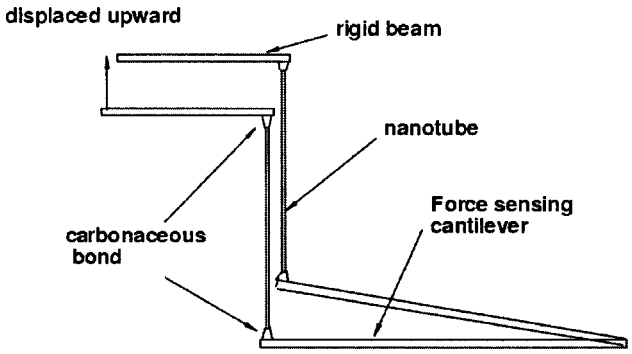

FIG. 2. An individual multiwalled carbon nanotube mounted between two opposing AFM tips.

The outer nanotubes in the experiments of Yu *et al.*[8] varied in length from 1.80 to 11 μm and their diameters varied from 13 to 36 nm; the multiwalled nanotubes consisted of 2–19 nested nanotubes. The smallest of the outer nanotubes had about 180 atoms around the circumference, and 24 000 atoms along the length, which corresponds to a total of 4.3×10^6 atoms. The largest outer nanotube consisted of approximately 53.8×10^6 atoms. Treating so many atoms would entail very long computations, so most of our studies were conducted on smaller models. In the initial simulations, a [20, 0] zigzag tube (the tube is labeled by the usual pair of integers $[n_1,n_2]$ (Ref. 23)) consisting of 840 atoms was considered. The dimensions were: radius 0.76 nm and length 4.24 nm. We also studied larger nanotubes to show that these results are essentially independent of size for the defect-free nanotube; these will be described later.

We first describe the molecular mechanics simulations. A single bond at the center of the tube was weakened by 10% in all molecular mechanics simulations except where noted. The motivation for weakening one bond is that the nanotube is a multiatom molecule and only a few defects are known that could serve as a nucleation site for the crack (except for the Stone-Wales dislocation[4] which we consider later). In our simulations, except where noted, there were no defects in the model, so the models were perfectly uniform. Strictly speaking, there is no reason for weakening one bond if we were only interested in zero-temperature behavior. However, our objective was to ascertain room temperature behavior where the velocities of the atoms are random and nonzero. The kinetic energy of these atoms follows a Boltzmann distribution, and thus as the potential energy nears the inflection point due to the applied force, some bonds will be stretched beyond the point of maximum force by the kinetic energy. The intent of the 10% imperfection is to model the effect of random velocities on the behavior at nonzero temperatures.

In our simulations, one end of the nanotube was axially displaced while the other end was fixed so that the nanotube was stretched. The applied force is computed by summing the interatomic forces for the atoms along the end of the nanotube where the displacement is prescribed. Instead of reporting a deflection and force, we report strain and a nominal stress. The strain is given by $\varepsilon=(L-L_0)/L_0$, where L_0 and L are the initial and current length of the nanotube, respectively. The stress is calculated from the cross-sectional

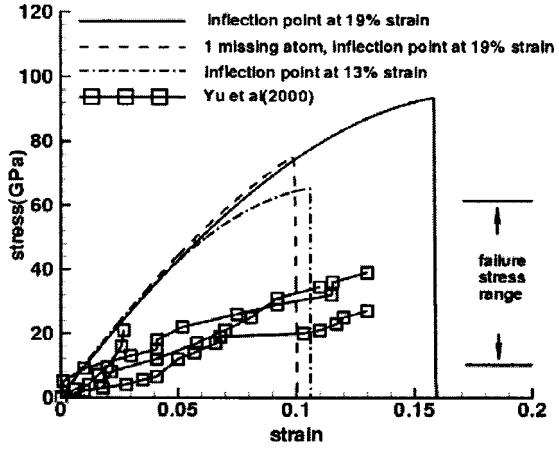

FIG. 3. Force-deflection curve for a model of zigzag nanotube as compared to experimental results (normalized to stress vs strain).

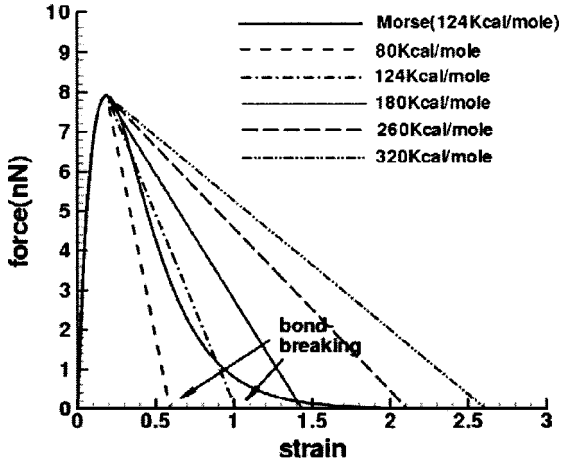

FIG. 4. Interatomic force-strain relationships for different separation energies for modified Morse potential.

area S ($S=\pi dh$, where d is the diameter of the nanotube and h is chosen as the interlayer separation of graphite, 0.34 nm, which has become customary).

For the Brenner potential, the nanotube in the molecular mechanics simulation failed at an elongation[2] of 28% and the tensile strength was 110 GPa. This agrees qualitatively with the computational results of Campbell, Brabec, and Bernholc[7] (~30%) but does not agree with the experiments of Yu *et al.*,[8] where most of the samples failed between 10% and 13% strain (one is as low as 2%) and the tensile strengths range from 11 to 63 GPa. From our studies, we inferred that the high fracture strain could be attributed to the camelback in the Brenner potential due to the cutoff function mentioned in the previous section.

With the modified Morse potential function of Eqs. (1)–(3), molecular mechanics simulations give a failure strain of 15.7% and a failure stress of 93.5 GPa. The normalized stress-strain results along with the experimental results of Yu *et al.*[8] are shown in Fig. 3. As can be seen, the failure strain is somewhat greater than the highest experimental value, while the failure stress is significantly higher. The computed stress exhibits a sudden drop to zero at failure, so the fracture can be considered brittle. Yu's experiments also show brittle fracture, for the reported force continues to increase until the final measurement, where the force suddenly drops to zero. Young's modulus for these experimental results is significantly below those previously reported (see beginning of this section). It is possible that some slippage occurred at the attachments for the high-strain cases reported in Yu *et al.*,[8] resulting in a decrease in the measured values of Young's modulus. Such slippage would also imply that the failure strains are smaller than reported.

To get a better insight into the relationship between fracture and separation energy, we varied the separation energy for the Morse function but kept the inflection point (i.e., the maximum of the interatomic force) unchanged. For this purpose, we used linear approximations to the Morse force field after 19% strain as shown in Fig. 4. These force fields with linear postpeak behavior are not intended for general applications, but are used here strictly to study the effect of varying the separation energy. Moreover, it has been noted often that potential functions are quite well described using universal functions such as Rydberg[24,25] and Morse[26] functions, for which the location of the inflection point and the separation energy are strongly connected. This means that realistic potential functions are a good deal less flexible than we have assumed in Fig. 4. However, although there may be some relationship between separation energy and the inflection point, we doubt it is as strong as indicated in the preceding, for there would then be no need for first-principles models.

Table I gives the failure strains of the nanotube for different separation energies. As before, one end was displaced axially to stretch the nanotube. In addition to the Morse potential, in which the inflection point (i.e., the peak force) occurs at 19% strain, we considered a potential with the inflection point at 13% strain. The constants for the modified Morse model are give in Table I. The temperature was considered to be 0 K. It can be seen from Table I that the failure strain depends very little on the separation energy but is strongly dependent on the location of the inflection point. The results for the nanotube with the modified Morse model with a 13% inflection point and 124 kcal/mol separation energy are also plotted in Fig. 3. It can be seen that the failure stress is only a little above the highest failure stress reported by Yu *et al.*[8] The failure strain is somewhat lower than the three specimens for which experimental stress-strain records are available, but the possible slippage in the experiments could explain this discrepancy. The secant Young's moduli at 5% strain for the two models are also given and are in close agreement with each other and the previously cited values.

We repeated some of these studies for a [60, 0] nanotube (separation energy of 124 kcal/mol) to check the effect of nanotube size on the failure behavior. The failure strain and stress were almost identical to those of the smaller nanotube models. Figure 5 shows the evolution of the crack in the tube. It can be seen that the bond-breaking spreads sideways after the initially weakened bond fails. The failure process is completed when all bonds around the circumference have failed. We found that once a single bond failed, no equilibrium solution could be found with a larger load, and that the failure process required very little additional displacement.

TABLE I. Failure strains of [20,0] nanotube for modified Morse potentials with various separation energies and interatomic force peaks at 19% and 13% strain.

Separation energy (Kcal/mol)	Inflection at 19% strain $D_e = 6.031\,05\times10^{-19}$ N m, $\beta = 2.625\times10^{10}$ m^{-1}, $E_{sec} = 0.85$ TPa		Inflection at 13% strain $D_e = 2.8949\times10^{-19}$ N m, $\beta = 3.843\times10^{10}$ m^{-1}, $E_{sec} = 0.81$ TPa	
	Failure strain (%)	Failure stress (GPa)	Failure strain (%)	Failure stress (GPa)
80	15.0	92.2	10.3	65
100	15.1	92.3	10.4	65.1
124	15.2	62.6	10.6	65.2
150	15.4	92.9	10.7	65.4
180	15.6	93.1	10.8	65.5
220	15.7	93.3	11.0	65.6
260	15.9	93.5	11.1	65.6
320	16.1	93.6	11.4	65.7

Thus the failure was highly brittle regardless of the size of the model.

We have considered a large range of separation energies because the potential energy function is highly uncertain for strains beyond the inflection point, and we wanted to examine whether the results depend on the separation energy. The simple interatomic potential used here is certainly not capable of describing the proper behavior of the system when bonds are broken, and indeed, breaking of the sp^2 bond in a carbon nanotube can result in a variety of phenomena that go beyond what our model can do. For example, new bonds could form between the dangling bonds on the carbon atom at the edge of the fracture region,[27] probably with rehybridization, and structural transformations such as the Stone-Wales transformation can take place in rings near the edge so as to seal the end of the fractured tube. Some of these phenomena will depend on the surroundings of the carbon nanotube, and temperature is also expected to play a role. Thus if fracture strength depended strongly on the separation energy, it would not be reasonable to model fracture with molecular mechanics. Fortunately, our results show a very weak dependence of fracture strain on the separation energy, so the shape of the potential surface after the inflection point cannot be important to fracture behavior. The simulations show that the failure strain of the nanotube is essentially independent of the separation energy and depends primarily on the inflection point of the interatomic potential.

According to Table I, the failure strains are about 15.5% for a large range of separation energies with the inflection at 19% strain. This failure strain of the nanotube is smaller than the strain at which a single interatomic force achieves its peak, 19%. This can be explained by the hexagonal molecular structure of the nanotube. As a consequence of the structure of the bonds, the strains in the longitudinal interatomic bonds are larger than the average strain in the nanotube. For an inflection point of 13%, the failure strains are around 10.8%. The ratio of the failure strain to the inflection strain (10.6%/13%) is almost identical to the other case (15.2%/19%).

As mentioned in the Introduction, atoms may be ejected from a nanotube in the TEM environment. We simulated this situation by removing a single atom and the three associated bonds in a zigzag nanotube. The modified Morse potential with a 19% inflection strain and 124 kcal/mol separation energy was used. The computed failure strain is 10% while failure stress is 74 GPa. The normalized force-deflection curve for this simulation is shown in Fig. 3. The force-deflection curve of this defective nanotube is almost identical to that of the defect-free nanotube until it fractures. However, fracture occurs at a substantially lower stress and strain than for the defect-free nanotube, and the fracture strain is below several of the values reported by Yu *et al.*[8] However, the fracture stress is still greater than all observed values.

We next examine the effect of the chirality on fracture. Yu *et al.*[8] were not able to measure the chirality of the outermost nanotubes, so we cannot compare the effect to experiments.

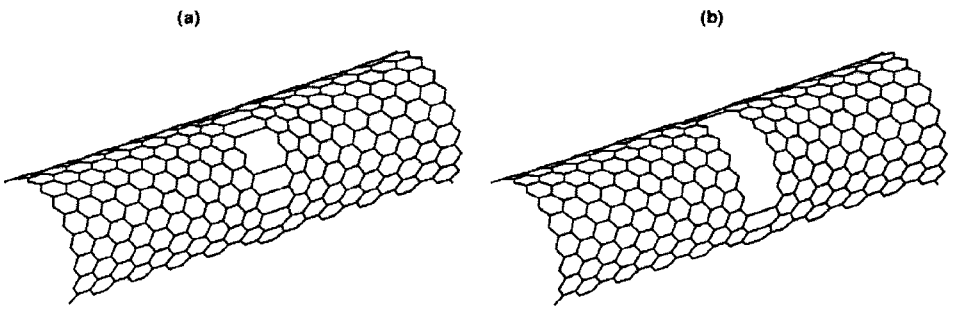

FIG. 5. Evolution of the crack in the nanotube.

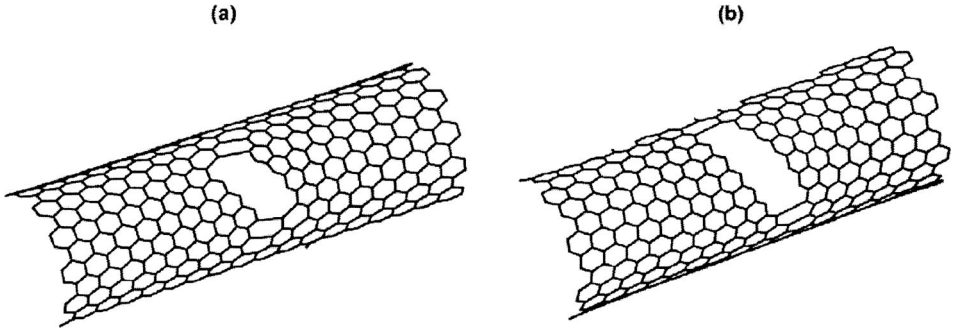

FIG. 6. Crack evolution in the (a) [12,12] armchair nanotube and (b) [16,8] chiral nanotube.

We examined three types of nanotubes in addition to the zig-zag nanotube: (1) [12, 12] armchair nanotube, (2) [16, 8] chiral nanotube, (3) [16, 4]chiral nanotube.

The modified Morse potential with the separation energy of 124 kcal/mol was used in all simulations. Molecular mechanics simulations with one-end displaced as before were made. Figure 6 shows the crack evolution for the chiral and armchair nanotube, showing that the failure pattern is similar to that of the zigzag nanotube. The computed force-deflection curves are shown in Fig. 7. It can be seen that the calculations predict a moderate dependence on the chirality of the nanotube on the strength. The computed failure strain of the [12, 12] armchair nanotube is 18.7%, and the failure strength is 112 GPa. Thus the armchair nanotube is stronger than the zigzag nanotube, and the strength of the [16, 8] nanotube (17.1% failure strain and 106 GPa failure stress) is between the two. The failure mode is brittle for all cases, with a rapid decrease in stress after the start of the fracture.

In order to ascertain the appropriateness of weakening a bond in the molecular mechanics studies, we made several molecular dynamics simulations without any weakened bonds. For a temperature T, the thermal energy is given by

$$E_{\text{thermal}} = C_p T, \tag{6}$$

where $C_p = 8.64\ \text{J mol}^{-1}\ \text{K}^{-1}$. A Boltzmann distribution is used for the velocities, which are related to the thermal energy by

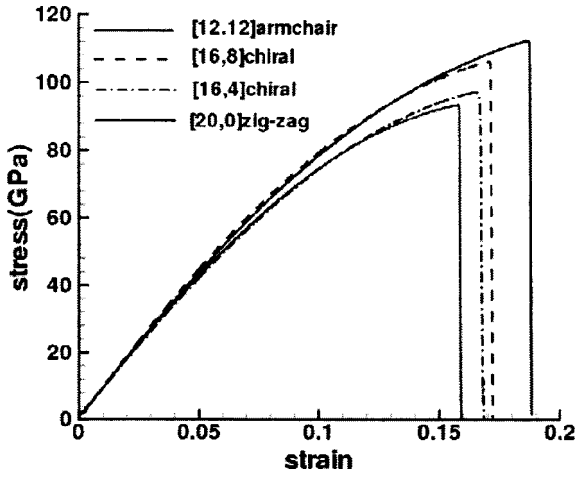

FIG. 7. Normalized force-deflection curves for nanotubes of different chiralities.

$$E_{\text{thermal}} = \frac{1}{2}\sum_{I=1}^{N}\sum_{i=1}^{3} m_I \nu_{iI}^2, \tag{7}$$

where N is the number of atoms, m_l is the mass of atom I, and ν_{iI} are the components of the velocity of atom I.

The modified Morse potential with an inflection point at 19% strain and 124 kcal/mol separation energy was used at temperatures of 200–400 K. The Yu *et al.*[8] experiments were completely static in a mechanical sense: the loads were applied over several minutes while the period of the lowest frequency a nanotube (length = 4.24 nm) is estimated to be 0.21 ps. In molecular dynamics simulations of essentially static phenomena, a common hazard is that if the loading (or prescribed displacement) is applied too quickly, stress-wave-like phenomena occur with considerable overshoot in interatomic forces. These can lead to spurious fracture. Applying the prescribed displacement from zero to the failure strain in a molecular dynamics simulation without inducing spurious fracture proved to be too expensive. Therefore we ran the simulation as follows:

(1) A molecular mechanics simulation was used to bring the nanotube to 12% tensile strain.

(2) The velocities due to temperature were applied to the atoms and the model was brought to steady state by integrating the momentum equations for the atoms in time (steady-state is often called equilibrium).

(3) The displacements at the end were prescribed to provide an extensional strain rate of 0.0072/ps.

In these molecular dynamics simulations, we found that the location of the crack was quite arbitrary and varied from simulation to simulation, but the scatter in the fracture strength was quite small. The nanotube failed at $(15.8\% \pm 0.3)\%$ strain at a stress of 93 ± 1 GPa. This compares quite well with the 15.8% strain and 93.5 GPa stress obtained from the molecular mechanics simulation with a 10% weakened bond.

One topological defect that has recently been identified theoretically is the 5/7/7/5 defect.[10] This defect corresponds to a 90° rotation of a C-C bond about its center as shown in Fig. 8, and is called a Stone-Wales transformation.[4] It results in two pentagons and two heptagons coupled in pairs. To study the effect of this defect on the behavior of the nanotube, we simulated a single defect at the center of the [12, 12] armchair nanotube by molecular dynamics. The displacement was prescribed at the end of the nanotube and the 124

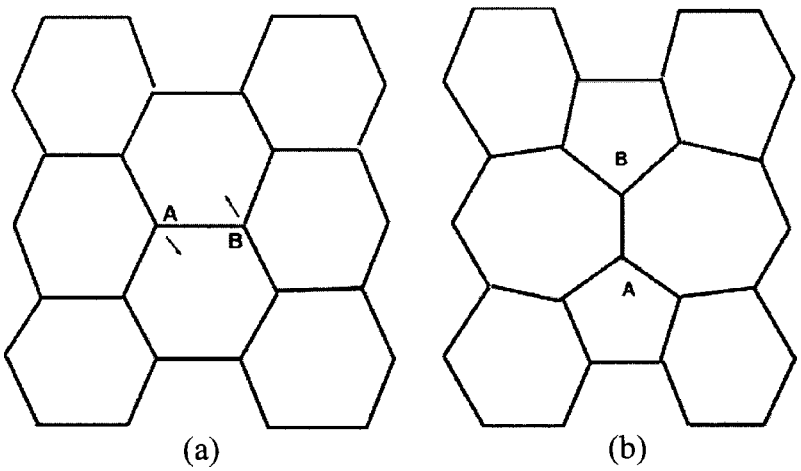

FIG. 8. Defect in (a) before rotation and (b) after rotation.

kcal/mol modified Morse potential was used. The failure strain is 14.3% and the failure stress is 97.5 GPa. Compared to the armchair nanotube with a weakened bond shown in Fig. 7, the 5/7/7/5 dislocation gives a somewhat lower failure strain and lower tensile strength. The fracture is still brittle.

The study of the 5/7/7/5 defect was repeated with an [40, 40] armchair nanotube. In this case the failure strain of the tube is 14.2% and the fracture is still brittle. So the size of the nanotube has little effect on the strength. Figure 9 shows that for the 5/7/7/5 dislocation, the maximum shear strain occurs in the $\pm(\pi/4)$ direction.[10] As can be seen from Fig. 9, the cracks grow in the direction of maximum shear.

IV. CONCLUSIONS

It has been shown that some of the salient features of the fracture behavior of carbon nanotube, such as the brittle character of the fracture and the magnitudes of fracture strains, can be explained by atomistic simulations. In these simulations, the range of failure strains of defect-free nanotubes was found to correspond roughly to observed values, and is in the range of 10%–16%. However, the predicted fracture stresses are too large. For a modified Morse potential that closely matches the Brenner potential in the 0–15% strain range, the failure stress is 93 GPa; for a potential with an inflection point at 13% strain, the failure stress is 65 GPa. The latter value is close to the highest value reported by Yu *et al.*[8]

A similar reduction in strength is observed when a defect is introduced by removing one atom and the associated bonds. It may be conjectured that all of the nanotubes in the experiments of Yu *et al.*[8] contain defects and that the large scatter in failure stress may be due to these defects.

It was shown that the fracture strain of extremely homogeneous systems with covalent bonds, such as the carbon nanotube, appears to be driven primarily by the inflection point in the interatomic potential, even when defects are included. The separation (dissociation) energy has little effect on the fracture strain. For fourfold differences in the separation energy, the failure stress only changes by 1%.

Nanotubes with several chiralities were also studied. Chirality appears to have only a moderate effect on the strength of nanotubes, with the failure stress varying from 93.5 to 112 GPa and the failure strain from 15.8% to 18.7%. In all cases the fracture was predicted to be brittle, which agrees with experiments.

Because of the homogeneity of multiatom molecules such

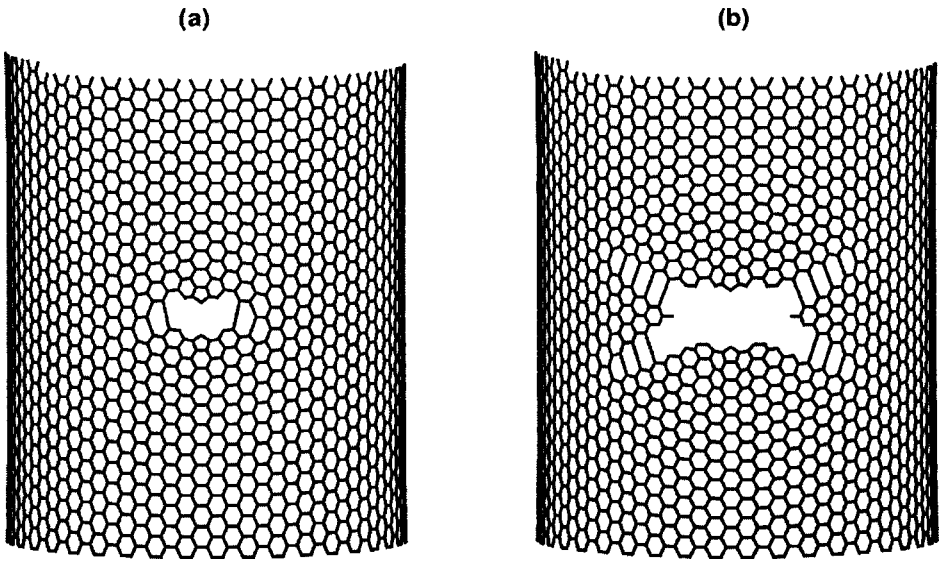

FIG. 9. Crack formation in the [40,40] armchair nanotube with 5/7/7/5 defect at (a) 12.7 ps and (b) 12.8 ps.

as the nanotube, it is difficult to postulate minor defects for nucleating a fracture. To provide a nucleation site for a crack in the defect-free nanotubes, we reduced the strength of a single bond by 10%. Our explanation for this artifact is that when the nanotube is near failure at nonzero temperature, because of the nonzero velocities of the atoms, some atoms would pass beyond the inflection point even in a perfect, homogeneous nanotube. This approach was verified by molecular dynamics studies.

We also studied the effects of missing atoms and 5/7/7/5 defects. The latter have small effects on strength but changed the failure pattern: the band of broken bonds occurs at an angle to the circumference of the nanotube. Nevertheless, the failure mode remained brittle. Even a single missing atom has a significant effect on strength, reducing it by about 25%. However, a missing atom also decreases the failure strain significantly, so the computed failure strains then underestimate the experimental results.

The application of atomistic models of active bonds such as carbon must generally be treated with caution. However, the great insensitivity of the results to dissociation energies provides some confidence that these models can be used for fracture studies of nanotubes in a variety of situations. The significant overprediction of experimentally measured failure strengths by simulations of defect-free models suggests that defects may play an important role in the fracture behavior of nanotubes.

ACKNOWLEDGMENTS

The support of the Army Research Office and National Science Foundation are gratefully acknowledged by the first two authors. G. S. acknowledges the supported of AFOSR MURI Grant No. F49620-01-1-0335. R. R. gratefully acknowledges the support of the NASA Langley Research Center for Computational Materials: Nanotechnology Modeling and Simulation Program.

*Email address: tedbelytschko@northwestern.edu

[1] S. Iijima, Nature (London) **56**, 354 (1991).
[2] S. Iijima, C. Brabec, A. Maiti, and J. Bernholc, J. Chem. Phys. **104**, 2089 (1996).
[3] B. I. Yakobson, C. J. Brabec, and J. Bernholc, Phys. Rev. Lett. **76**, 2511 (1996).
[4] M. R. Falvo, G. J. Clary, R. M. Taylor II, V. Chi, F. P. Brooks, Jr., S. Washburn, and R. Superfine, Nature (London) **389**, 582 (1997).
[5] J. Despres, E. Daguerre, and K. Lafdi, Carbon **33**, 87 (1995).
[6] R. S. Ruoff and D. Lorents, Bull. Am. Phys. Soc. **40**, 173 (1995).
[7] M. P. Campbell, C. J. Brabec, and J. Bernholc, Comput. Mater. Sci. **8**, 341 (1997).
[8] M. F. Yu, O. Lourie, M. J. Dyer, K. Moloni, T. F. Kelly, and R. S. Ruoff, Science **287**, 637 (2000).
[9] M. B. Nardelli, B. I. Yakobson, and J. Bernholc, Phys. Rev. Lett. **81**, 4656 (1998).
[10] B. I. Yakobson, Appl. Phys. Lett. **72**, 918 (1998).
[11] M. B. Nardelli, B. I. Yakobson, and J. Bernholc, Phys. Rev. B **57**, 4277 (1998).
[12] R. Chang, Int. J. Fract. Mech. **6**, 111 (1970).
[13] P. C. Gehlen and M. F. Kanninen, 587, edited by M. F. Kanninen (McGraw-Hill, New York, 1970).
[14] J. E. Sinclair and B. R. Lawn, Proc. R. Soc. London, Ser. A **329**, 83 (1972).
[15] O. A. Shenderova, D. W. Brenner, A. Omeltchenko, X. Su, and L. H. Yang, Phys. Rev. B **61**, 3877 (2000).
[16] A. Omeltchenko, J. Yu, R. K. Kalia, and P. Vashishta, Phys. Rev. Lett. **78**, 2148 (1997).
[17] B. W. Smith and D. E. Luzzi, in *The Physics of Electronic and Atomic Collisions*, edited by Louis J. Dubé, J. Brian A. Mitchell, J. William McConkey, and Chris E. Brion, AIP Conf. Proc. No. **360** (AIP, Woodbury, NY, 1995).
[18] F. Banhart, Rep. Prog. Phys. **62**, 1181 (1999).
[19] D. W. Brenner, Phys. Rev. B **42**, 9458 (1990).
[20] G. Van Lier, C. Van Alsenoy, V. van Doren, and P. Geerlings, Chem. Phys. Lett. **326**, 181 (2000).
[21] J. P. Lu, Phys. Rev. Lett. **79**, 1297 (1997).
[22] J. P. Salvetat, G. A. D. Brriggs, J. M. Bonard, R. R. Bacsa, A. J. Kulik, T. Stockli, N. A. Burnham, and L. Forro, Phys. Rev. Lett. **82**, 944 (1999).
[23] C. T. White, D. H. Robertson, and J. W. Mintmire, Phys. Rev. B **47**, 5485 (1993).
[24] J. R. Smith, T. Perry, A. Banerjea, J. Ferrante, and G. Bozzolo, Phys. Rev. B **44**, 6444 (1991).
[25] D. Vogtenhuber and R. Podloucky, Phys. Rev. B **55**, 10 805 (1997).
[26] J. L. Graves and R. G. Parr, Phys. Rev. A **31**, 1 (1985).
[27] A. Maiti, Phys. Rev. Lett. **331**, 21 (2000).